Received May 10, 2015, accepted June 10, 2015, date of publication July 2, 2015, date of current version July 16, 2015.

Digital Object Identifier 10.1109/ACCESS.2015.2452576

On the Spatial Distribution of Base Stations and Its Relation to the Traffic Density in Cellular Networks

SHENG ZHOU[1], (Member, IEEE), DONGHEON LEE[1,2], BINGJIE LENG[1], XUAN ZHOU[3,4], HONGGANG ZHANG[3], (Senior Member, IEEE), AND ZHISHENG NIU[1], (Fellow, IEEE)

[1]Tsinghua National Laboratory for Information Science and Technology, Department of Electronic Engineering, Tsinghua University, Beijing 100084, China
[2]SK Telecom, Seoul 100-999, Korea
[3]Zhejiang University, Hangzhou 310027, China
[4]Huawei Technologies, Shenzhen 518108, China

Corresponding author: S. Zhou (sheng.zhou@tsinghua.edu.cn)

This work was supported in part by the National Basic Research Program of China (973 Program) under Grant 2012CB316000, in part by the National Science Foundation of China under Grant 61201191, Grant 61321061, Grant 61401250, and Grant 61461136004, and in part by Hitachi Ltd., Japan.

ABSTRACT The spatial distribution of base stations (BSs) and traffic demands is essential for efficient network planning and BS sleeping, which are key elements of green cellular networking. This paper investigates their statistics, relation, and modeling, based on large-scale measurement data from commercial cellular networks. The spatial distribution of BSs shows not only high nonuniformity over a region but also diverse patterns in different regions, and thus the widely used homogeneous Poisson point process can only approximate the BS patterns in a specific small area. Therefore, the inhomogeneous PPP (IPPP), in particular, the Cox point process with spatially varying intensity is used to model the BS distribution over any spatial scale. To model the intensity distribution of the IPPP, we exploit the relation, shown to be sublinear, between the BS distribution and the peak hour (PH) traffic density, based on the finding that the PH traffic density can be approximated by a log-normal distribution. Finally, we propose a spatial modeling framework for network simulations, and discuss potential applications of the proposed spatial distribution model of the BS patterns and the PH traffic density.

INDEX TERMS Spatial analysis and modeling, spatial pattern of base stations, traffic density, inhomogeneous Poisson point process, Cox point process.

I. INTRODUCTION

The explosive development of wireless cellular networking incurs ever increasing network deployment cost and energy consumption [1], [2]. As a result, for the green paradigm shift of cellular networks, efficient network planning [3] and intelligent base station (BS) sleeping mechanisms [4], [5] are in urgent need. The basic idea of either green network deployment or BS operation is matching the network resources to the spatial and temporal variations of the traffic [3], which in the first place requires the knowledge of the BS distribution pattern and its relation to the traffic-demand fluctuations.

A. RELATED WORK

Models of spatial patterns and traffic load of BSs are separately studied in various existing works [6]–[15]. The spatial distribution of traffic load has been studied in the literature for 2G [6], [7] and 3G cellular networks [8], [9], respectively. Among the very first studies, ref. [6] proposes a general model based on log-normal distribution to characterize the spatial traffic variations on the cell level. More recently, mixtures of log-normal distributions are shown to have better model precision in [7]. For 3G data networks, ref. [8] relates subscribe behaviors and the cell traffic variations, and the authors also find small traffic load correlations among adjacent cells. In [9], probabilistic models are further used to estimate the loads on all the BSs based on actual measurements only on a small subset of BSs.

Spatial processes for modeling spatial patterns of BSs are studied in [10]–[15]. The homogeneous Poisson point process (HPPP) [18], in which the intensity is constant over space, is widely used for modeling and simulation of the spatial structure of BS deployment [10] due to its simplicity

and tractability. Based on real data sets of BS deployments in many cities worldwide, a study [11] has shown that the HPPP model is more accurate than hexagonal grid model in terms of coverage analysis. Recently, there have been some efforts to look for a realistic model of BS patterns based on real measurements. Guo and Haenggi [12] show that the Strauss process, the Poisson hard-core process, and the perturbed triangular process can be used to accurately model the spatial structure of BS deployments. In [13] and [15], it is shown that the Geyer saturation process is capable of modeling the spatial structure of a Wi-Fi network and macro-cell BSs, respectively. In [14], it is shown that BS deployments in an urban and a rural area can be fitted by Matern cluster process and the Strauss hard-core process, respectively. In [16], the authors use the Ginibre point process to model random phenomena of BS positions with repulsion, where repulsion means that the node locations of a real deployment usually appear to form a more regular (or more clustered) point pattern than the HPPP.

However, the results of above works are divergent and there does not exist a generally accepted model. In addition, most studies of spatial traffic load and BS distribution are performed independently, and there are few works revealing the relation between the positions of BSs and the traffic distribution. Note that Michalopoulou *et al.* [7] point out that there are negative correlations between the traffic load and the coverage area of a cell. In [17], a parameterized statistical model is proposed to characterize the correlation between user and BS locations, however the model has not been validated with real world data. In summary, the realistic modeling of the spatial distribution of both BS locations and traffic demand, and the relation between them, remain largely unknown.

B. CONTRIBUTIONS and METHODOLOGY

Based on large-scale measurement data from commercial cellular networks, the main contribution of this paper is characterizing the spatial distribution of BSs with Cox point process, of which the parameters are obtained via the in depth investigation on the relation between BS intensity and the traffic demand distribution. Based on the statistical analysis, a modeling framework is proposed to generate both the traffic demand and BS locations, with extensive applications for planning and operating cellular networks. The methodology used in this paper and the paper organization are overviewed as follows.

Since the real BS deployments are highly non-uniform and different countries have different urban planning and population distributions, we are not aiming at finding the most adequate stationary spatial point process for modeling BS locations. Rather, in this paper, we focus on providing a flexible method to model BS locations based on a large-scale measurement data set from commercial GPRS/EDGE cellular networks deployed in a major east province of China, as described in Section II.

In Section III, we first find that the intensity of BS deployments can only be approximated by a HPPP in a specific small area, as the BS intensity is varying over a relatively large area. We then show that an inhomogeneous PPP (IPPP), whose intensity varies with locations, can be used for modeling BS locations for the large area. In order to model the spatial patterns of BSs, we employ the Cox point process [18], which is a generalization of the IPPP where the intensity function is random. Then, modeling the intensity function of the Cox point process is a critical part. Since the network planning, which locates BSs and adjusts their configurations, is closely related to peak hour (PH) traffic demand, we exploit the relation between BS intensity and PH traffic demand to model the intensity function.

In Section IV, we measure the traffic density defined as the traffic load per unit area. In our previous work [19], only the distribution of the traffic density at 9 p.m. of a week day is analyzed. We extract PH traffic load of every cell during two weeks and calculated the PH traffic density for representing PH traffic demand. We also find that the distribution of PH traffic density can be approximated by a log-normal distribution.

The relation between the BS deployment and the PH traffic density is obtained through regression analysis in Section V. In particular, we show that a sublinear model and a linear model is proper for an urban and rural area, respectively. By exploiting the findings previously mentioned, in Section VI-A we propose a spatial modeling framework which generates both the PH traffic density and BS locations based on the Cox point process. Finally in Section VI-B we discuss the potential applications of the proposed modeling framework, especially for green cellular communications.

II. DATA SET

The locations of BSs are obtained from GPRS/EDGE networks deployed in one east province in China. The target area of the measurement is a metropolitan area of 160km$\times$180km including urban, suburban, and rural areas. The population of the city in the metropolitan area is more than 9 million. In this paper, a dense urban area and a rural area depicted in Fig. 1 and 2 are selected to investigate BS locations and the PH traffic density. The locations of BSs are obtained by converting from longitude, latitude geodetic coordinates to X, Y cartesian coordinate (we assume the heights of BSs are zero as we do not have the terrain information). There are about 6297 cells in the target area.

In recent years, China has undergone rapid urbanization and dramatic population growth in urban area and thus shows a variety of spatial structures among various cities. Planning of cellular networks is closely related to the structure of a city and population. Hence, while the placement of BSs in an urban area is highly dense where the radii of small size cells is even several tens of meters, the radii of large cells in the rural area reaches to a few kilometers as shown in Fig. 1 and 2.

We have also collected traffic records of packet-switched data traffic from EDGE/GPRS networks in the same region

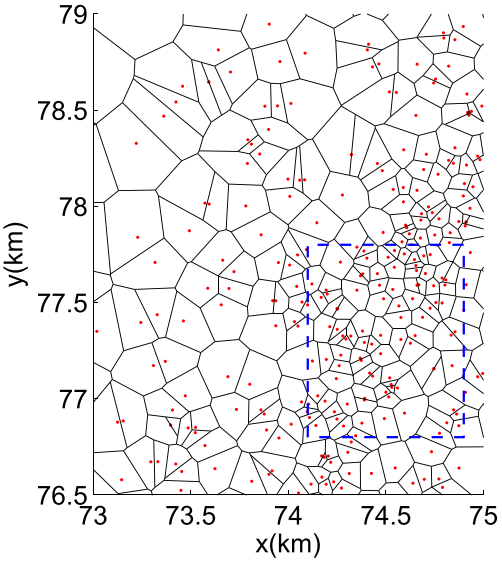

FIGURE 1. Base station locations (dots) and corresponding Voronoi cells (lines) in a urban area. The dashed rectangular area and the whole area are denoted by 'UA1' and 'UA2', respectively.

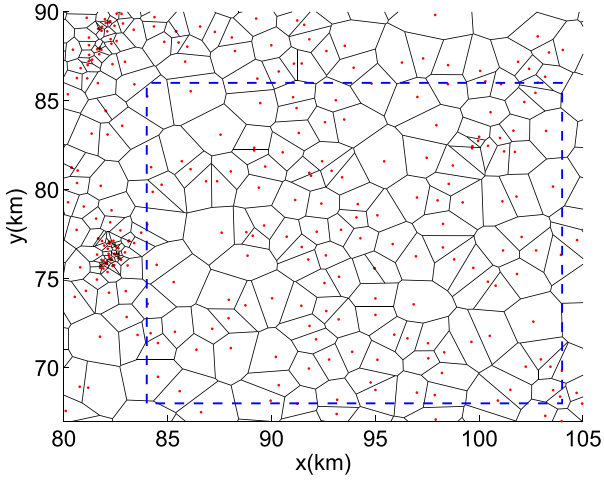

FIGURE 2. Base station locations (dots) and corresponding Voronoi cells (lines) in a rural area. The area in the blue rectangular and the whole area are denoted by 'RA1' and 'RA2', respectively.

during May 1-14 in 2013. It is measured in the unit of kilobyte (KB) that each BS actually transmitted during a one-hour time interval. For the modeling of the spatial traffic distribution, we introduce the traffic density (traffic load per unit area) which can be easily calculated by using the information from BSs. In our previous work [19], the distribution of the traffic density at an instantaneous time t is analyzed, while in this paper we consider the PH traffic load, which is closely related to BS site planning.

III. SPATIAL DISTRIBUTION OF BS LOCATIONS

In this section, we check whether the spatial distribution of BSs can be described by the most commonly used PPP [18]. After we find that fitting with HPPP only holds for small areas, we turn to fit the general BS distribution with IPPP. Let us consider a spatial point process X which is the set of all points (the BS locations in a target area $A \subset R^2$) $X = \{x_1, x_2, \ldots, x_n\}$. In the PPP [18], [21], the number of points $N(A)$ in any region A is a Poisson random variable with the non-negative intensity $\lambda(x)|A|$, $\forall x \in A$ and $|A|$ is the area of the region A. When λ is a constant, the distribution is generally called HPPP, otherwise it is called IPPP.

A. FITTING BS DEPLOYMENTS BY A HOMOGENEOUS PPP

Figure 3(a) illustrates the distribution of the number of BSs in UAi ($i = 1, 2$) and the fitting by Poisson distributions with parameter $\lambda_{\mathrm{UA}i}|A_{\mathrm{UA}i}|$ for UAi, where $|A_{\mathrm{UA}i}|$ is the test area randomly taken inside UAi. The number of BSs in $0.8\mathrm{km} \times 1\mathrm{km}$ area of UA1 is 95 and thus λ_{UA1} is 118.75. The number of BSs in $2\mathrm{km} \times 2.5\mathrm{km}$ area of UA2 is 267 and thus λ_{UA2} is 53.4, which are easily obtained by the maximum likelihood estimator of the homogenous PPP. The test area of $0.2\mathrm{km} \times 0.2\mathrm{km}$, where the number of BSs is counted, is randomly chosen inside UAi in every experiment. The empirical probability distribution function (PDF) obtained

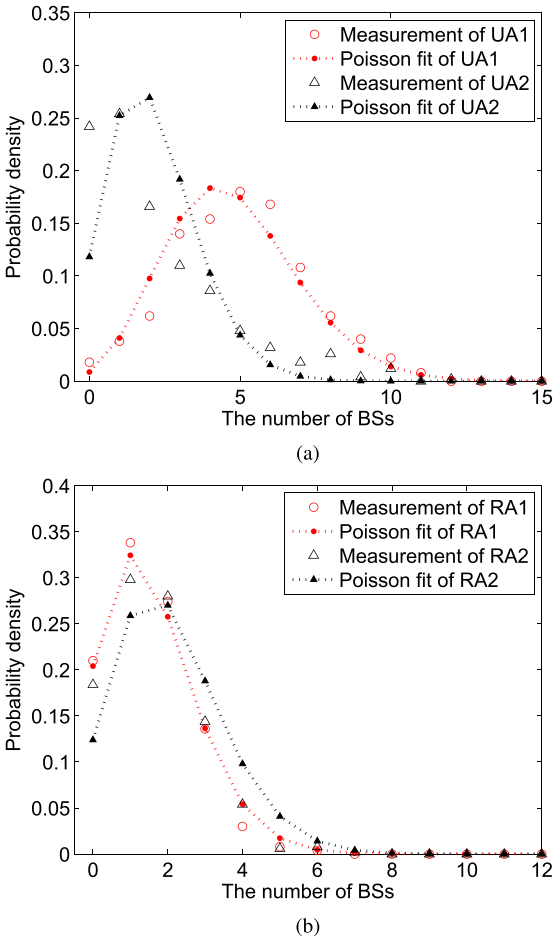

FIGURE 3. Fit test of HPPPs: the distribution of the number of BSs and the Poisson distribution with intensity (a) $\lambda_i^{(U)}|A_i^{(U)}|$ in UAi and (b) $\lambda_i^{(R)}|A_i^{(R)}|$ in RAi.

from 500 times experiments and the Poisson distribution with the intensity 118.75×0.2^2 and 53.4×0.2^2 for each region are also depicted in Fig. 3(a).

The number of BSs in 20km $\times$ 18km area of RA1 is 143 and thus λ_{RA1} is 0.3972. The number of BSs in 25km $\times$ 23km area of RA2 is 300 and thus λ_{RA2} is 0.5217. The test area of 2km $\times$ 2km is selected. Figure 3(b) shows the empirical PDFs and the Poisson distributions with the intensity 0.3972×2^2 and 0.5217×2^2 for each region.

In the selected areas of UA1 in Fig. 3(a) and RA1 in Fig. 3(b), where the spatial distribution is regarded as stationary, we observed that the empirical PDF is well fitted by a Poisson distribution. If a region is classified into several small areas with the same characteristics, e.g., city center, residential area, business district, parks and recreation, and so on, then the spatial distribution of BS locations may be stationary within each small area. However, the spatial distribution of BSs in UA2 and RA2 is highly non-uniform and cannot be fitted by a single HPPP.

B. HOMOGENEOUS L-FUNCTION TEST

Ripley's $K(r)$ function can be used to precisely evaluate whether a point pattern is fitted by a HPPP, and this function is used to describe a point pattern, estimate statistical parameters, and fit models [22]. The $K(r)$ function of a stationary spatial point process is estimated by

$$\hat{K}(r) = \frac{1}{|A|\lambda^2} \sum_i \sum_{i \neq j} I(d_{ij} \leq r), \tag{1}$$

where d_{ij} is the distance between point x_i and x_j and $I(\cdot)$ is the indication function. If the point pattern is approximately HPPP, i.e., also known as complete spatial randomness (CSR), $\hat{K}(r)$ should be approximately πr^2.

On the other hand, the L-function, which is widely used instead of K-function in practice, is defined as $L(r) = \sqrt{K(r)/\pi}$ [18]. We used the software "R" and "spatstat" package [23] to calculate the L-function. Figure 4 and 5 plot the empirical L-function with different edge correction methods for each region respectively. We see that the L-function of UA1 is overlapping with the CSR's L-function which is consistent with the results in the previous section. However, the L-functions of UA2 lie above the CSR L-function, which means the spatial distribution of BSs in UA2 is clustered (non-HPPP). The L-function of RA1 is also almost matched with the CSR curve, but that of RA2 is obviously deviated from the CSR line.

From the previous discussions, we know that only the spatial statistics of selected small areas with common characteristics (e.g., business district, residential area) can be regarded as stationary since spatial variations are generally severe across broad geographic regions. *Therefore, we conclude that the BS locations only in a relatively small area with common characteristics can be modeled by a homogeneous PPP.*

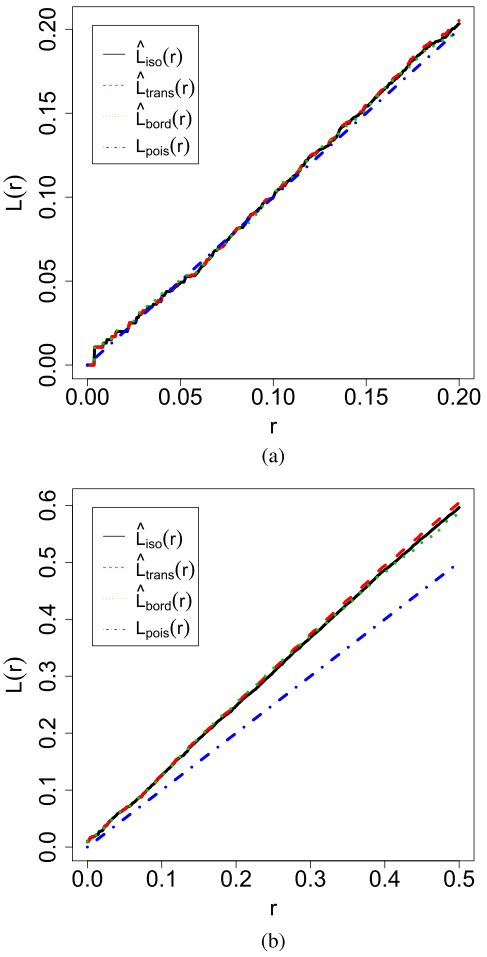

FIGURE 4. L-function test for the urban areas: $\hat{L}_{iso}$, $\hat{L}_{trans}$, $\hat{L}_{bord}$, and $\hat{L}_{pois}$ indicate a L-function with edge correction of the Ripley's isotropic correction, the border method, the translation correction, and of a HPPP (see the manual of the package "spatstat" at [23]). (a) UA1. (b) UA2.

C. ESTIMATION OF INTENSITY FUNCTION FOR THE IPPP

So far, many spatial models for nodes of wireless networks, such as mobile terminals, access points, and BSs, assume spatial homogeneity. However, in reality, the distribution of node locations is often inhomogeneous over space, i.e. they can be described by an inhomogeneous point process with non-constant intensity $\lambda(x)$ for all $x \in A$. Since the intensity function is rather irregular depending on various regions, we investigate the probability distribution of the intensity function.

The classic approach to estimate the intensity function is based on kernel methods. For the sake of simplicity, we use the box kernel function [18] for the estimator, where the side of square box has length h. The bandwidth h determines the smoothness of surfaces, i.e., a larger h leads to smoother surfaces. The bandwidth h for UA2 and RA2 is set to 0.24 and 1.5, respectively.

Figure 6 and 7 show estimates of the intensity function and its probability distribution in UA2 and RA2, respectively. In Fig. 6(a), we can see that the value of the intensity

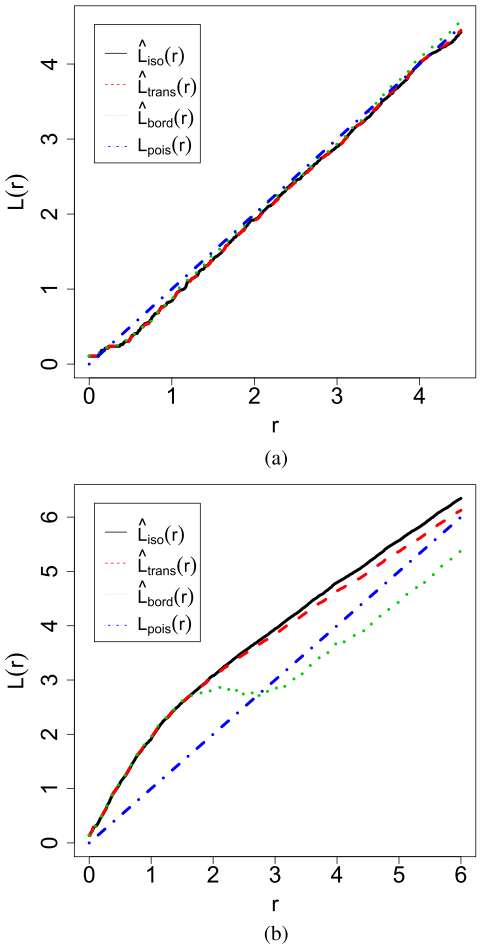

FIGURE 5. L-function test for the rural areas: $\hat{L}_{iso}$, $\hat{L}_{trans}$, $\hat{L}_{bord}$, and $\hat{L}_{pois}$ indicate a L-function with edge correction of the Ripley's isotropic correction, the border method, the translation correction, and of a HPPP (see the manual of the package "spatstat" at [23]). (a) RA1. (b) RA2.

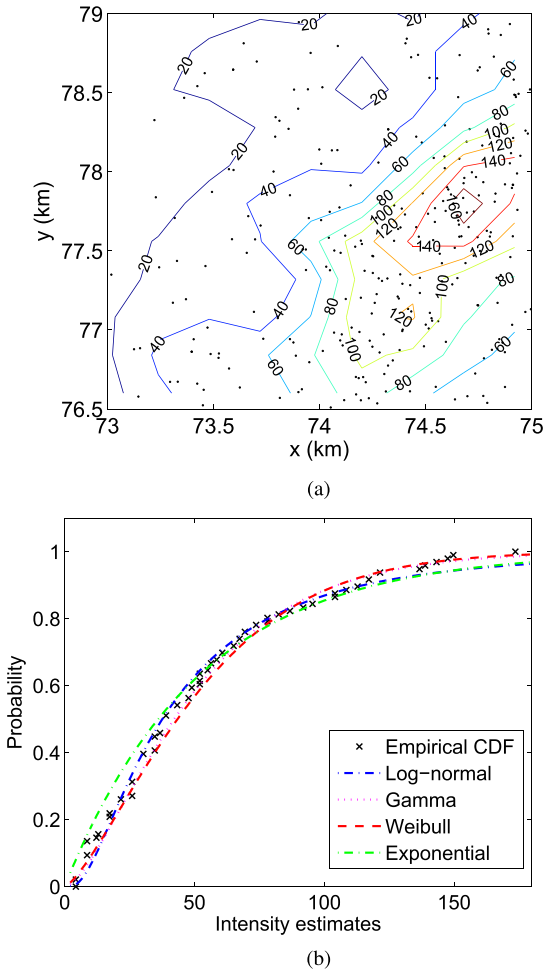

FIGURE 6. The estimation of intensity function with bandwidth $h = 0.24$km: (a) contour plot and (b) the CDF of intensity estimates in UA2 (dense urban area).

function gradually decreases from right to left across the region. The distribution of the estimates $\lambda(x)$ is positively skewed: skewness is 1.0567 and Kurtosis is 3.3985. The log-normal, gamma, Weibull, and exponential distribution are examined to fit the empirical distribution of the estimates. The cumulative distribution function (CDF) of the estimates and the distribution fittings for UA2 are depicted in Fig. 6(b). The Kolmogorov-Smirnov test (K-S test) is employed to check for goodness-of-fit of the empirical data. The K-S test results show that all the distributions cannot be rejected at the 5% significance level. The measured K-S test statistic, which is the maximum distance between the reference distribution and the empirical distribution, for the log-normal, gamma, Weibull, and exponential distribution are 0.0901, 0.0714, 0.0609, and 0.1334, respectively. Hence, the Weibull distribution shows the best fit for the intensity function of urban areas. The estimated value of the scale and the shape parameter of the Weibull distribution are 56.9756 and 1.3599, respectively.

In Fig. 7, there is a sudden variation in the intensity function at the left side of the figure. This causes that the K-S test rejects all the distributions. The mixture distribution should be required to accurately fit the significantly varying intensity function. The skewness and the Kurtosis of the values of the intensity function is 3.5953 and 16.6841, respectively. The K-S statistic of the log-normal distribution (0.1345) shows the best fit. The estimated value of the location and the scale parameter (the mean and standard deviation of the variable's natural logarithm) of the log-normal distribution is -0.8928 and 0.6890, respectively.

In our experiments, other distributions (the gamma and exponential distribution) also occasionally show better fit for the intensity functions in other regions. However, the Weibull and log-normal distributions are seen to be more flexible to fit many types of spatial patterns. Both the Weibull and log-normal distribution are widely used to describe the skewed data. In our tests, the Weibull distribution tends to overestimate the head part of the empirical distribution while the log-normal distribution does in the tail part on the same empirical data. This is the reason why the Weibull distribution is better for fitting the smoothly varying surfaces (the gentle slope in the CDF curve), whereas the log-normal distribution

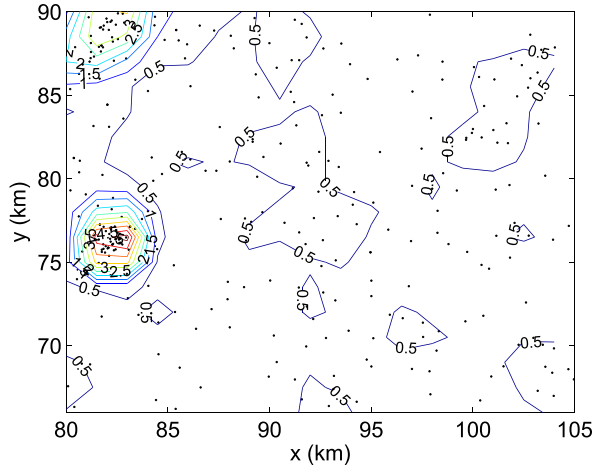

(a)

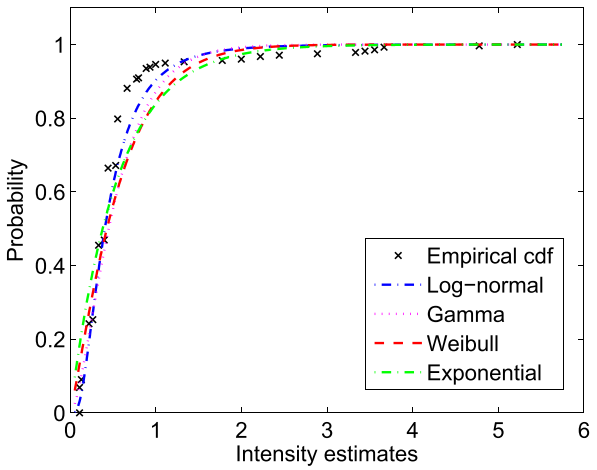

(b)

FIGURE 7. The estimation of intensity function with bandwidth $h = 1.5$km: (a) contour plot and (b) the CDF of intensity estimates in RA2 (rural area).

is better for fitting the significantly varying surfaces (the steep slope in the CDF curve).

D. INHOMOGENEOUS L-FUNCTION TEST

The inhomogeneous K-function $K_{inhom}(r)$ is the generalization of the K-function introduced in Section III-A [26]. Analogously, if X is an IPPP with intensity function $\lambda(x)$, then $K_{inhom}(r) = \pi r^2$. The inhomogeneous K-function is computed by

$$\hat{K}_{inhom}(r) = \frac{1}{|A|} \sum_i \sum_{j \neq i} \frac{I(d_{ij} \leq r)}{\lambda(x_i)\lambda(x_j)}, \tag{2}$$

This calculation requires the intensity function estimates $\hat{\lambda}(x)$ for $\lambda(x_i)$ and $\lambda(x_j)$. Figure 8 and 9 show the computed inhomogeneous L-functions $L_{inhom}(r) = \sqrt{K_{inhom}(r)/\pi}$ of BS locations in UA2 and RA2, respectively, based on the intensity estimates obtained in the previous section. The envelopes in Fig. 8 and 9 are obtained

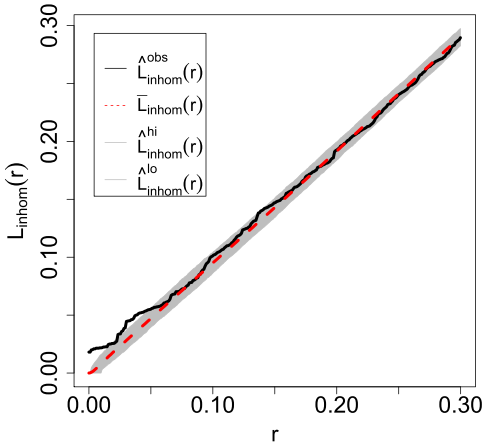

FIGURE 8. Empirical inhomogeneous L-function obtained from BS locations in UA2 and envelops (the shadowed area between $\hat{L}^{hi}_{inhom}$ and $\hat{L}^{lo}_{inhom}$) of $L_{inhom}(r)$ computed from 600 realizations of an IPPP. The dashed line $\bar{L}_{inhom}(r)$ is the average value of the L-functions of 600 realizations of the fitted IPPP.

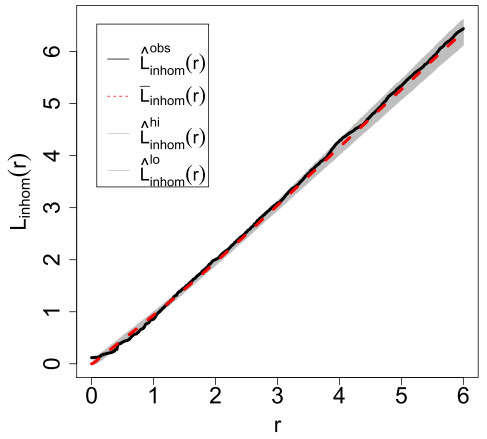

FIGURE 9. Empirical inhomogeneous L-function obtained from BS locations in RA2 and envelops (the shadowed area between $\hat{L}^{hi}_{inhom}$ and $\hat{L}^{lo}_{inhom}$) of $L_{inhom}(r)$ obtained from 600 realizations of an IPPP. The dashed line $\bar{L}_{inhom}(r)$ is the average value of the L-functions of 600 realizations of the fitted IPPP.

from 600 simulated realizations of the IPPP, taking the 30-th highest and 30-th lowest values of simulated L-functions, with intensity estimates $\hat{\lambda}(x)$ the same as the intensity estimates depicted in Fig. 6 and 7. Since the observed inhomogeneous L-functions of UA2 and RA2 lies almost inside the envelope, we conclude that *BS locations over a relatively large area can be modeled by an IPPP*.

IV. THE DISTRIBUTION OF PEAK HOUR TRAFFIC DENSITY

Denote cell traffic for the ith cell at time t by $\psi_{i,t}$. Cell traffic is the aggregate traffic volume which the BS of the cell actually transmitted to all the users in the cell during the one-hour time period between t and $t+1$. Peak hours, which are the time when traffic volume is at its peak during a certain period in each cell, are different depending on the region in

which a cell is located [8], [25]. Hence, we extract PH cell traffic which is the highest volume of the cell traffic during the consecutive 14 days of each cell: $\Psi_i = \max_t\{\psi_{i,t}\}$ for all $i = 1, \ldots, n$, where $t = 1, \ldots, 24 \times 14$.

The PH traffic density is measured in a grid basis. Assume that the target area is the two-dimensional $J \times K$ grid of equally-spaced points. The pixel $p_{j,k}$, where $j = 1, \ldots, J$ and $k = 1, \ldots, K$, contains the PH traffic density $\mathbf{Z} = \{Z[j,k]), j = 1, \ldots, J, k = 1, \ldots, K\}$. We first calculate cell traffic per cell area, $R_i = \Psi_i / D_i$, where D_i indicates the area of the ith Voronoi cell. Then each pixel is assigned to R_i of the nearest cell i and thus the PH traffic density is finally obtained. The size of each pixel in the grid is set to 0.01 km and 0.1 km for urban and rural areas, respectively, which is much smaller than the average cell radius. The map of the PH traffic density ($ln(\mathbf{Z})$) of UA2 and RA2 are depicted in Fig. 10.

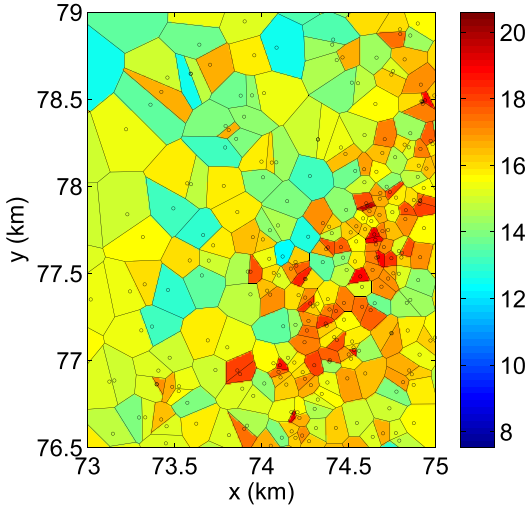

(a)

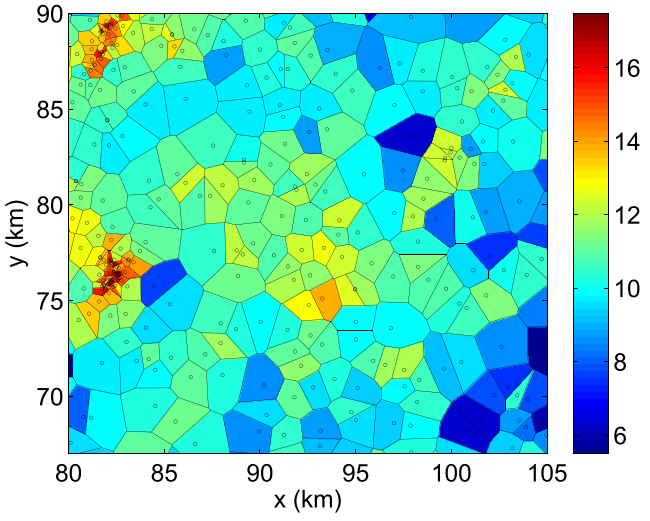

(b)

FIGURE 10. The logarithm of peak hour traffic density. (a) UA2. (b) RA2.

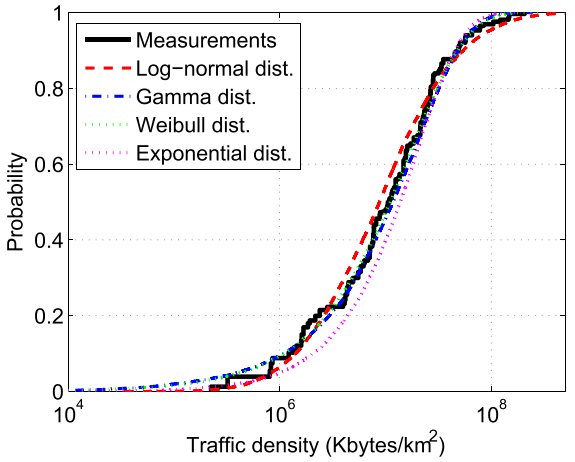

(a)

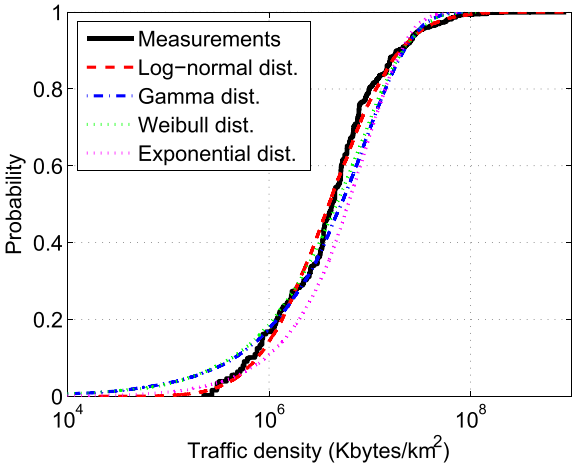

(b)

FIGURE 11. The distribution of the PH traffic density in urban areas. (a) Downlink, UA1. (b) Downlink, UA2.

A. DISTRIBUTION FITTING

Figure 11 shows the empirical CDFs of the downlink PH traffic density $\mathbf{Z}$ and its fitting with log-normal, Weibull, gamma, and exponential distributions. The K-S test results show that all the distributions should be rejected at the 5% significance level. However, in terms of the K-S statistics, the log-normal distribution shows the best fitting performance (0.0425, 0.0468 for uplink, downlink in UA1, and 0.0419, 0.0772 for uplink, downlink in UA2). The CDFs of the PH traffic density of RA1 and RA2 are depicted in Fig. 12. In the same manner like urban areas, the K-S statistics of log-normal distribution shows the least value (0.0422, 0.0514 for uplink, downlink in RA1, and 0.0270, 0.0454 for uplink, downlink in RA2). Therefore, we conclude that *the peak hour traffic density can be approximated by a log-normal distribution.* This fact can be exploited to develop the spatial modeling framework of the PH traffic density, which is discussed in more details in Section VI-A1.

The location (μ) and the scale (σ) parameters of log-normal distributions for each region obtained by the maximum likelihood estimation are listed in Table 1.

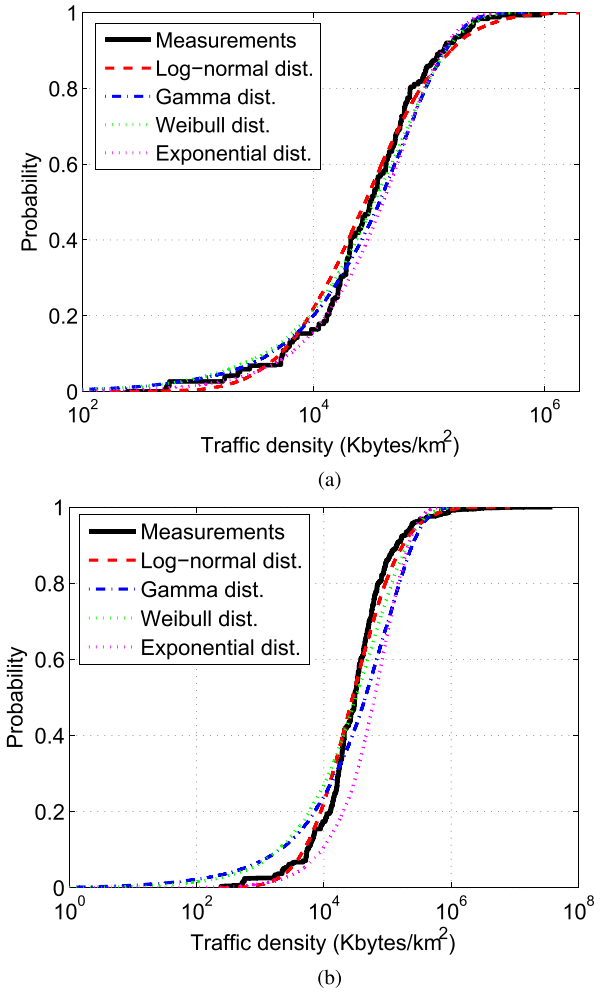

FIGURE 12. The distribution of the PH traffic density in rural areas. (a) Downlink, RA1. (b) Downlink, RA2.

TABLE 1. Parameters of the log-normal distribution fitting.

	Uplink		Downlik	
	μ	σ	μ	σ
UA1	14.7007	1.6076	15.999	1.4116
UA2	13.8401	1.4288	15.1738	1.2744
RA1	8.7604	1.559	10.2496	1.3034
RA2	8.7435	1.564	10.2637	1.3885

B. SPATIAL CORRELATION MODELING BY VARIOGRAM MODEL

Another important observation is that PH traffic density maps in Fig. 10 represent some degree of correlations between adjacent cells. Cell traffic collected at BS locations is actually related to the value of an underlying continuous spatial traffic demand. Cell traffics of neighboring BSs at the same time have correlations and thus the traffic density has also spatially auto-correlated distribution. In spatial modeling of the PH traffic density, it is important to include spatial correlations of the traffic density.

In geostatistics, the varigoram model is used for obtaining the second moments of spatial data [20], [21]. The (semi-)variogram $\gamma(\mathbf{h})$ of a stochastic process Y is the variances of differences: $2\gamma(\mathbf{h}) = E[\{Y(X) - Y(X+\mathbf{h})\}^2]$ for all lags $\mathbf{h}$, which describes how the spatial correlation decays as a function of the lag $\mathbf{h}$. The sample variogram of the PH cell traffic per cell area $R(x_i)$ is computed by

$$\hat{\gamma}(\mathbf{h}) = \frac{1}{2|N(\mathbf{h})|} \sum_{N(\mathbf{h})} \{R(X) - R(X')\}^2, \tag{3}$$

where the set of all pairs of points separated by lag vector $\mathbf{h}$ is denoted by $N(\mathbf{h}) = \{(X, X'), \|X - X'\| = \mathbf{h}\}$.

We have tested several variogram models but select the exponential variogram model, which is simple and shows a good agreement empirically. The exponential variogram model is defined as $\gamma(\mathbf{h}) = v(1 - \exp(-\mathbf{h}/r))$, where the parameter v is the variance of the process and r decides the decay rate of correlation. The parameter r is estimated by using the weighted least squares estimator [21]. Figure 13 shows the obtained sample variogram from the logarithm of the PH traffic density ($\ln(R_i)$) of UA2 and the fitted exponential variogram as an example.

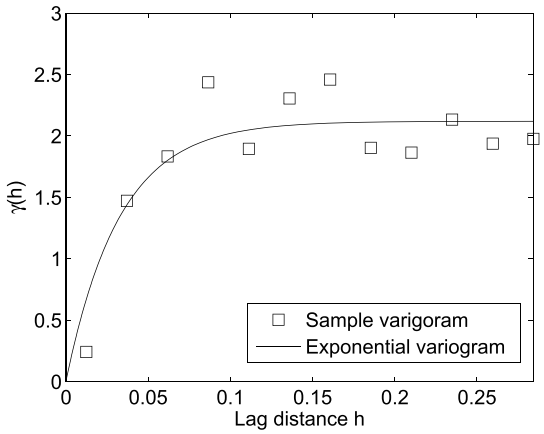

FIGURE 13. The sample varigoram of the PH traffic density of UA2 and the fitted exponential semi-variogram.

Note that $\gamma(\mathbf{h}) = 0$ means that the correlation is 1, otherwise, the larger its value is, the less spatial correlation is observed. In Fig. 13, the variogram reaches its upper bounds known as the *sill*: it is same with the variance v of the stochastic process. The finite lag distance at which a variogram reaches its sill is called *range*. It also means that beyond this range, the PH traffic of the two positions becomes almost irrelevant. The measured range of UA1, UA2, RA1, and RA2 are 0.0154, 0.0870, 1.7139, and 5.3722 km, respectively. The parameter r for the exponential variogram model is typically given by one third of the range.

V. THE RELATION BETWEEN BS DEPLOYMENTS AND TRAFFIC DENSITY

The PH traffic density can be exploited to determine the intensity function of the spatial BS distribution, since BSs tend to be more densely deployed at a place where traffic demand is high, and vice versa. In order to model a spatial pattern of BSs

with an intensity function estimated by the PH traffic density, it is essential to know their *relation* quantitatively beforehand.

A. PEAK HOUR TRAFFIC DENSITY AND CELL AREA

The number of deployed BSs and BS locations are closely related to the traffic density of a target area. Many small cells are likely to be deployed in the area of high traffic density as it can be observed in Fig. 10.

Traffic per cell (cell traffic) and cell area exhibit some degree of negative correlations in countrywide scale [7]. It means that the higher the traffic load, the smaller cell sizes. We investigate the correlation between the PH traffic density and cell area as shown in Fig. 14. We check correlations between the traffic density and cell area and observe strong negative correlations, which shows the Spearmans's correlation coefficient of -0.6099 and the Pearson's correlation coefficient of -0.2200.

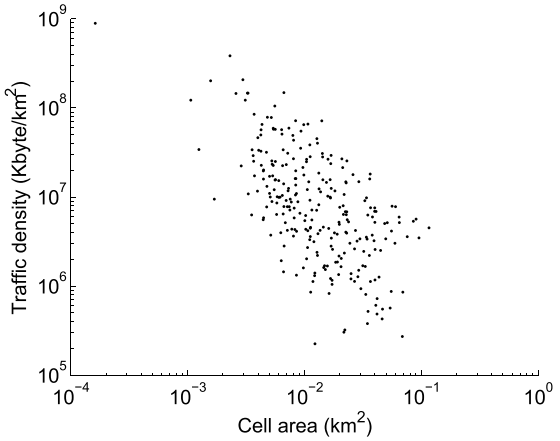

FIGURE 14. A scatter diagram of traffic density versus cell area in UA2.

B. THE INTENSITY OF BS DEPLOYMENTS AND PEAK HOUR TRAFFIC DENSITY

The relation between the PH traffic density and the number of BSs in UA1 is depicted in Fig. 15. We take a square sliding window W of 0.35 km $\times$ 0.35 km in UA2 and calculate the aggregate traffic load $T(W) = d\sum_j \sum_k Z[j,k]$, where j and k are the index of pixels inside the window W, and d is the area of a pixel. Denote the intensity by $\lambda(W)$ inside the window W. Regression analysis is used to model the relation between the BS distribution intensity estimates and the aggregate traffic load. Since the intensity function cannot increase to infinity at high values of traffic load, we model the regression function as a sublinear function as follows:

$$\lambda(W) = a\exp(-b/T(W)), \tag{4}$$

where the fitting parameters a and b are obtained by the simplex search method. The obtained parameters are provided in Table 2. The relation model (4) is obtained from estimating the relation between the intensity estimates and the mean values of traffic load (circles in Fig. 15) for each intensity values.

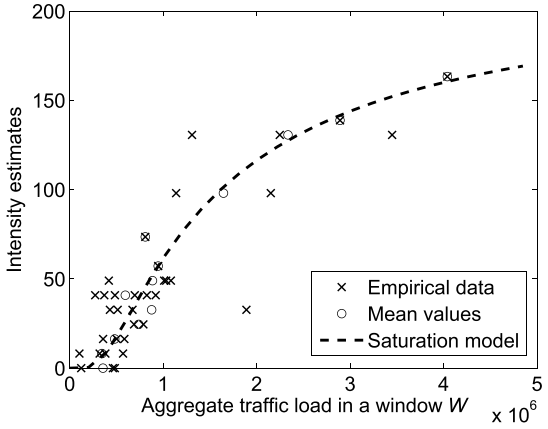

FIGURE 15. The relation between the intensity function and the average traffic load per window W in UA2.

TABLE 2. Parameters of the relation model for modeling.

Urban area(UA2)			Rural area(RA1)		
a	b	r' (km)	c	d	r' (km)
219.987	1274675.964	0.147	0.279	3.248×10^{-7}	0.571

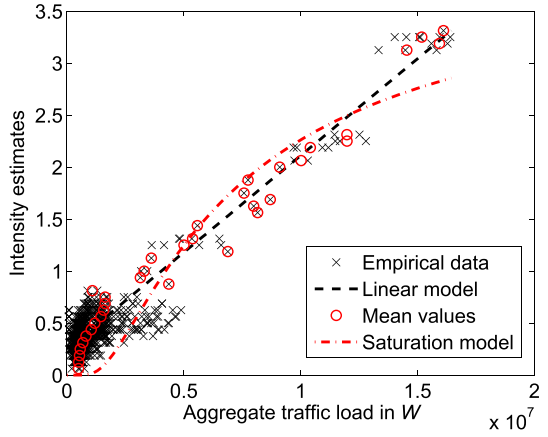

FIGURE 16. The relation between the intensity function and the average traffic load per the window W in RA2.

Figure 16 shows the relation graph for RA2. Since the distribution of BS locations and traffic density varies significantly at the left side in RA2 (there is actually a small town), there is a clear discontinuity around 0.7 of intensity estimates. In addition, the results of modeling performance, e.g., K-function graph comparison, show that the proposed modeling fails to successfully replicate the significantly varying surface. Hence, we select RA1 to investigate the relation for a rural area. The relation graph for RA1 is depicted in Fig. 17. We select a linear regression model $\lambda(W) = cT(W)+d$ for spatial modeling of the rural area and estimate the relation from the points in Fig. 17 by using the iterative re-weighted least squares algorithm. The parameters c and d are also given in Table 2.

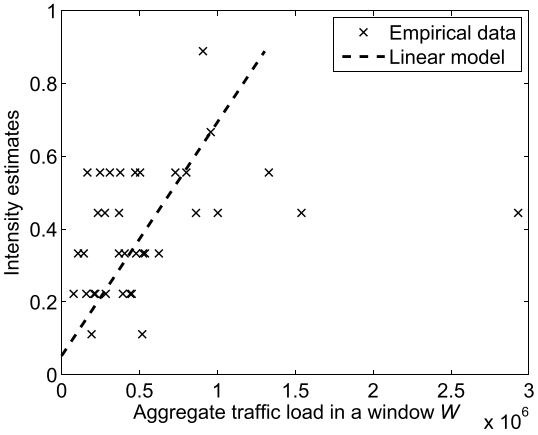

FIGURE 17. The relation between the intensity function and the average traffic load per window W in RA1.

VI. APPLICATIONS OF THE PROPOSED MODELS

In this section, we illustrate potential applications of the proposed modeling on the BS location distribution and the PH traffic density. Firstly a spatial modeling framework is introduced as an effective way of providing close-to-real BS locations and traffic densities, for simulating the mobile network performance. Then we will briefly introduce how to apply the proposed models for BS planning optimization and dynamic BS sleeping control.

A. SPATIAL MODELING FRAMEWORK FOR NETWORK SIMULATIONS

The spatial modeling framework proposed here provides a simulation method to generate both inhomogeneous BS deployments and the PH traffic density by using the variogram and the spatial Gaussian model [27] as widely used in geostatistics. The framework exploits findings presented in the previous sections, i.e., the possibility of the use of a homogeneous PPP for a specific small area, the log-normally distributed traffic density, and the relation between the intensity function and the traffic density.

The framework is based on Cox point process [28] which consists of the first step of intensity function generation and the second step of IPPP construction. The details are as follows.

1) GENERATE THE MAP OF THE PH TRAFFIC DENSITY BY A GAUSSIAN SPATIAL PROCESS

Let $\mathbf{Z} = \{Z[j,k], j = 1,\ldots,J, k = 1,\ldots,K\}$ denote the PH traffic density generated on a two-dimensional $J \times K$ grid like the same manner in Section IV.

As mentioned, the PH traffic density can be approximated by a log-normal distribution. Hence, we can represent the PH traffic density Z by

$$Z[j,k] = e^{(\mu + S[j,k])}, \tag{5}$$

where the stationary Gaussian spatial process $\mathbf{S} = \{S[i,j], j = 1,\ldots,J, k = 1,\ldots,K)\}$ follows a zero-mean multivariate Gaussian distribution with covariance function $\rho(h) = \mathrm{Cov}[S[j,k]S[j',k'])]$, where h is the distance between pixel $[j,k]$ and $[j',k']$. The Gaussian spatial process $S[j,k]$ should be scaled by using μ and σ given in Table 1 so that it has the same distribution with the empirical data. The specification of the covariance function $\rho(\mathbf{h})$ for all lags $\mathbf{h}$ determines the smoothness of the resulting Gaussian spatial process $\mathbf{S}$ and is given by

$$\rho(\mathbf{h}) = \exp\{-(\mathbf{h}/r)\}, \tag{6}$$

where v is set to 1 since the variance can be adjusted in (5).

In Fig. 18(a), a generated sample of the log-transformed PH traffic density, i.e., $\mathbf{S}$, is depicted by the color map.

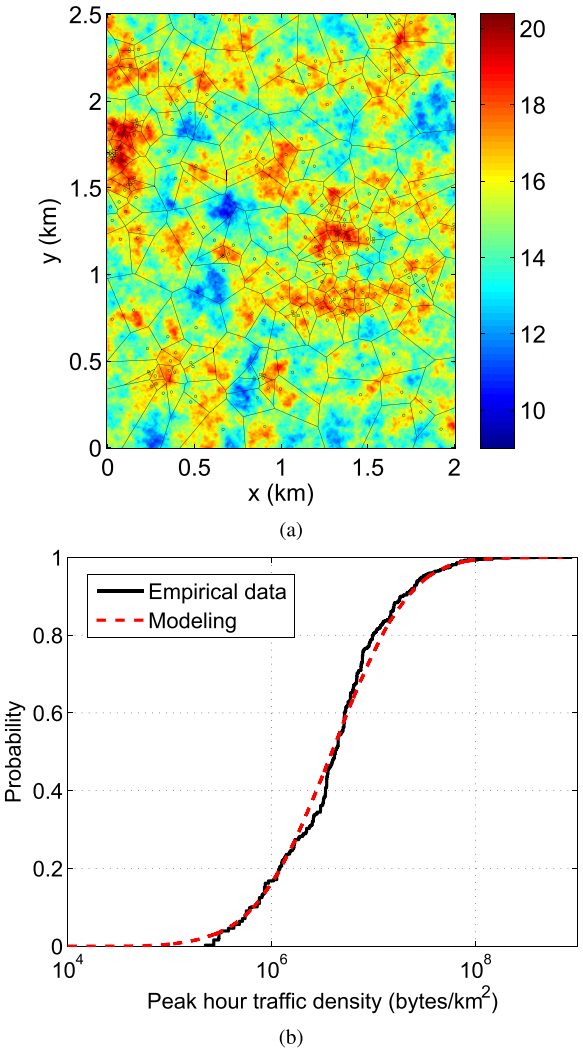

FIGURE 18. The PH traffic density modeling: (a) a sample of the generated PH traffic density; (b) the distribution of the empirical data and a sample generated by modeling.

2) GENERATING BS LOCATIONS

After generating the grid map of the PH traffic density (Kbytes/km^2) by (5), the number of BSs can be obtained by using the relation model (4). The traffic density map is partitioned into $J_s \times K_s$ disjoint square segments of the same

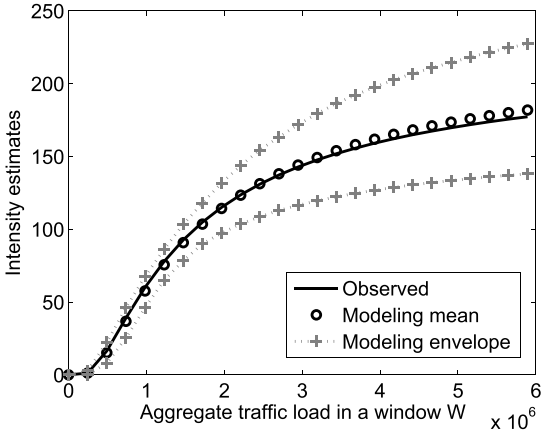

FIGURE 19. The relation between the intensity function and the aggregate traffic load.

size $s \times s$, where $J_s = \lfloor J/s \rfloor$ and $K_s = \lfloor K/s \rfloor$. The segments are denoted by $\mathbf{W} = \{W_{u,v}, u = 1, \ldots, J_s, v = 1, \ldots, K_s\}$ and the aggregate traffic load (Kbyte) in each segment $W_{u,v}$ is given by

$$T(W_{u,v}) = d \sum_{j=1}^{s} \sum_{k=1}^{s} Z[m_1 + j, m_2 + k], \tag{7}$$

where $m_1 = (u-1)s$, $m_2 = (v-1)s$, and d is the area of a pixel. After calculating the aggregate traffic load $T(W_{u,v})$, the intensity $\lambda(W_{u,v})$ is directly obtained from the saturation relation model for urban areas and the linear relation model for rural areas. From the result of Section III, the spatial distribution of BS deployments of a specific region can be modeled by an IPPP. Hence, we generate spatial points by a thinning method of IPPP simulation [18] with the intensity $\lambda(W_{u,v})$ for all segments $\mathbf{W}$.

The performance of the proposed spatial modeling method is carried out by comparing the distribution of the PH traffic density, the intensity function of BS deployments with those of empirical data of UA2. The model simulation of an urban area has been implemented by choosing $d = 0.01$km, $s = 20$. It reproduces both BS deployments and the PH traffic density which are statistically the same with those of UA2. The parameter r for the exponential variogram given in Table 2 is adjusted to $r' = 6r$ for UA2, which is optimized through extensive simulations. A generated random sample of the Gaussian spatial process (the logarithm of the PH traffic density) and BSs are depicted in Fig. 18(a). As can be seen, higher intensity function is estimated at higher traffic density areas. Figure 18(b) shows that the CDF of a sample of PH traffic density matches that of the empirical PH traffic density of UA2 very well. Figure 19 shows the intensity estimates versus the aggregate traffic load per segment obtained from 600 realizations of PH traffic density and BS locations. From Fig.18–20, the observed curve lies within the modeling envelope and the mean of the sublinear regression functions shows a good agreement with that of the empirical data.

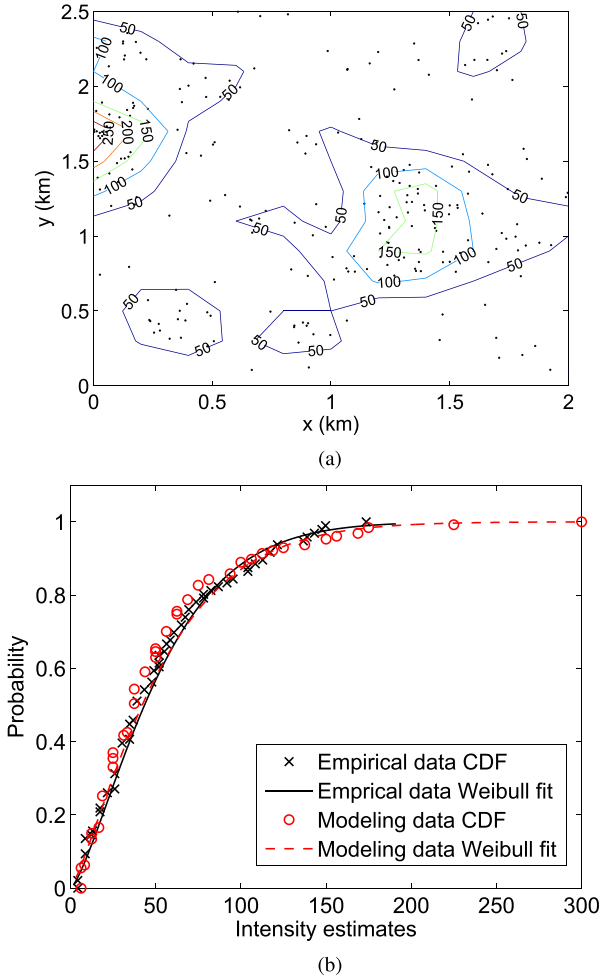

FIGURE 20. An inhomogeneous distribution of BS deployments: (a) the contour graph of the intensity estimates and (b) the distribution comparison.

B. BS PLANNING AND DYNAMIC BS SLEEPING

The basic idea of applying the proposed model is to check whether the BS density of a given area deviates severely from the relation to the traffic density, as predicted by (4). For network planning, it generally indicates that some new sites should be deployed, while for dynamic BS sleeping, it can trigger the actions to put some BSs into sleep or to wake up some sleeping BSs. Note that the performance of these mechanisms can in turn be simulated based on the spatial modeling framework previously introduced.

1) BS PLANNING

The operator can train the proposed model by determining the parameters a and b given in (4) periodically for every roughly septated regions, e.g., similar size as UA2 for dense urban areas and as RA2 for rural areas. At the beginning of each planning period, the operator can further divide every region with finer spatial granularity into small segments of the same size. Denote each segment as $W_{u,v}$. By counting the number of BSs, one gets the measured BS density in the segment $\lambda(W_{u,v})$. The operator can also measure the average

aggregated PH traffic in this segment, denoted by $\bar{T}(W_{u,v})$. The deviation of the BS density to the measured traffic PH is then given by

$$\Delta_{u,v} = \lambda(W_{u,v}) - a\exp(-b/T(W_{u,v})), \quad (8)$$

With all $\Delta_{u,v}$ on hand, the operator is able to select those negative $\Delta_{u,v}$ with large absolute values $|\Delta_{u,v}|$. Candidate mechanisms include: Sort $\Delta_{u,v}$, and then choose X segments with smallest $\Delta_{u,v}$ (should be negative); Comparing $\Delta_{u,v}$ with certain threshold, i.e., if $\Delta_{u,v} < \xi$, for a given $\xi > 0$, the segment is chosen. For those selected segments, the operator can further put efforts on deciding the number of new BSs to deploy and the best sites of the new BSs, via conventional BS planning methods. The size of the segments will tradeoff the BS deployment efforts by conventional methods with the model prediction precision, and thus should be optimized, which serves as a valuable future research direction.

2) DYNAMIC BS SLEEPING

When the traffic load in certain areas of the network is low, some BSs serving those areas can be put into sleep mode in order to save energy [3]–[5]. Most existing approaches perform in a centralized way to coordinate the sleeping and waking up actions of BSs. However, for densely deployed network, this may put heavy overhead to the network controller, and thus distributed sleeping decision, e.g., probability-based BS sleeping mechanisms [29] are preferable in dense networks. By using the proposed model, similar to the BS planning case, the operator should track the deviation in a finer time granularity, denoted by $\Delta^t_{u,v}$ at time t. Then the operator can assign a BS sleeping/waking up probability for each segment, denoted by $P_s(\Delta^t_{u,v})$ as a function of $\Delta^t_{u,v}$. Designing appropriate $P_s(\Delta^t_{u,v})$ also serves as a promising future research topic.

VII. CONCLUSION

In this paper, a new spatial modeling framework is proposed for the BS patterns and the PH traffic density based on a spatial analysis on real measurement data of commercial cellular networks. Our findings show that HPPP is only capable of modeling BS patterns in a specific small area, but IPPP is required to model diverse spatial patterns of BS deployments for a relatively large area in general. In order to model the intensity function of IPPP, we analyze the spatial distribution of the PH traffic density and its relation with the intensity function of BS locations. It is shown that the PH traffic density can be accurately fitted by a log-normal distribution. In addition, we find that it exhibits spatial correlations which can be evaluated by an exponential variogram model. We also observe that the sublinear model and the linear model are appropriate for the relation in an urban area and a rural area, respectively. This framework can be used to reproduce various inhomogeneous distributions of BS patterns and the corresponding PH traffic density together, which can be applied to realistic simulations of cellular networks. Moreover, applications for BS planning and dynamic BS sleeping can be developed based on the modeling framework and are worth future research efforts. Another direction of future research is to apply the proposed methodology to analyze the spatial patterns of heterogeneous networks, consisting of small cells with different radio access technologies.

REFERENCES

[1] Y. Chen, S. Zhang, S. Xu, and G. Y. Li, "Fundamental trade-offs on green wireless networks," *IEEE Commun. Mag.*, vol. 49, no. 6, pp. 30–37, Jun. 2011.
[2] G. Auer *et al.*, "How much energy is needed to run a wireless network?" *IEEE Wireless Commun.*, vol. 18, no. 5, pp. 40–49, Oct. 2011.
[3] Z. Niu, "TANGO: Traffic-aware network planning and green operation," *IEEE Wireless Commun.*, vol. 18, no. 5, pp. 25–29, Oct. 2011.
[4] E. Oh, B. Krishnamachari, X. Liu, and Z. Niu, "Toward dynamic energy-efficient operation of cellular network infrastructure," *IEEE Commun. Mag.*, vol. 49, no. 6, pp. 56–61, Jun. 2011.
[5] Z. Niu, Y. Wu, J. Gong, and Z. Yang, "Cell zooming for cost-efficient green cellular networks," *IEEE Commun. Mag.*, vol. 48, no. 11, pp. 74–79, Nov. 2010.
[6] R. Rathgeber, "Spatial traffic distribution in cellular networks," in *Proc. 48th IEEE VTC-Spring*, May 1998, pp. 1994–1998.
[7] M. Michalopoulou, J. Riihijarvi, and P. Mahonen, "Towards characterizing primary usage in cellular networks: A traffic-based study," in *Proc. IEEE DySPAN*, May 2011, pp. 652–655.
[8] U. Paul, A. P. Subramanian, M. M. Buddhikot, and S. R. Das, "Understanding traffic dynamics in cellular data networks," in *Proc. IEEE INFOCOM*, Apr. 2011, pp. 882–890.
[9] U. Paul, L. Ortiz, S. R. Das, G. Fusco, and M. M. Buddhikot, "Learning probabilistic models of cellular network traffic with applications to resource management," in *Proc. IEEE Int. Symp. DYSPAN*, Apr. 2014, pp. 82–91.
[10] J. G. Andrews, F. Baccelli, and R. K. Ganti, "A tractable approach to coverage and rate in cellular networks," *IEEE Trans. Commun.*, vol. 59, no. 11, pp. 3122–3134, Nov. 2011.
[11] C.-H. Lee, C.-Y. Shih, and Y.-S. Chen, "Stochastic geometry based models for modeling cellular networks in urban areas," *Wireless Netw.*, vol. 19, no. 6, pp. 1063–1072, 2013.
[12] A. Guo and M. Haenggi, "Spatial stochastic models and metrics for the structure of base stations in cellular networks," *IEEE Trans. Wireless Commun.*, vol. 12, no. 11, pp. 5800–5812, Nov. 2013.
[13] J. Riihijärvi and P. Mähönen, "Modeling spatial structure of wireless communication networks," in *Proc. IEEE INFOCOM*, Mar. 2010, pp. 1–6.
[14] Q. Ying, Z. Zhao, Y. Zhou, R. Li, X. Zhou, and H. Zhang, "Characterizing spatial patterns of base stations in cellular networks," in *Proc. IEEE/CIC Int. Conf. Commun.*, Oct. 2014, pp. 490–495.
[15] D. B. Taylor, H. S. Dhillon, T. D. Novlan, and J. G. Andrews, "Pairwise interaction processes for modeling cellular network topology," in *Proc. IEEE GLOBECOM*, Dec. 2012, pp. 4524–4529.
[16] N. Deng, W. Zhou, and M. Haenggi, "The Ginibre point process as a model for wireless networks with repulsion," *IEEE Trans. Wireless Commun.*, vol. 14, no. 1, pp. 107–121, Jan. 2015.
[17] M. Mirahsan, R. Schoenen, and H. Yanikomeroglu, "HetHetNets: Heterogeneous traffic distribution in heterogeneous wireless cellular networks," *IEEE J. Sel. Areas Commun.*, to be published.
[18] J. Illian, A. Penttinen, H. Stoyan, and D. Stoyan, *Statistical Analysis and Modelling of Spatial Point Patterns*. New York, NY, USA: Wiley, 2008.
[19] D. Lee, S. Zhou, X. Zhong, Z. Niu, X. Zhou, and H. Zhang, "Spatial modeling of the traffic density in cellular networks," *IEEE Wireless Commun.*, vol. 21, no. 1, pp. 80–88, Feb. 2014.
[20] N. Cressie, *Statistics for Spatial Data*, vol. 900. New York, NY, USA: Wiley, 1993.
[21] M. Sherman, *Spatial Statistics and Spatio-Temporal Data: Covariance Functions and Directional Properties*. New York, NY, USA: Wiley, 2010.
[22] P. M. Dixon, "Ripley's K function," in *Encyclopedia of Environmetrics*, vol. 3. New York, NY, USA: Wiley, 2002, pp. 1796–1803.
[23] A. Baddeley and R. Turner, "Spatstat: An R package for analyzing spatial point patterns," *J. Statist. Softw.*, vol. 12, no. 6, pp. 1–42, 2005.
[24] P. Diggle, "A kernel method for smoothing point process data," *J. Roy. Statist. Soc. C (Appl. Statist.)*, vol. 34, no. 2, pp. 138–147, 1985.

[25] J. Reades, F. Calabrese, and C. Ratti, "Eigenplaces: Analysing cities using the space–time structure of the mobile phone network," *Environ. Planning B, Planning Design*, vol. 36, no. 5, pp. 824–836, 2009.
[26] A. J. Baddeley, J. Møller, and R. Waagepetersen, "Non- and semi-parametric estimation of interaction in inhomogeneous point patterns," *Statist. Neerlandica*, vol. 54, no. 3, pp. 329–350, 2000.
[27] P. J. Diggle, J. A. Tawn, and R. A. Moyeed, "Model-based geostatistics," *J. Roy. Statist. Soc. C (Appl. Statist.)*, vol. 47, no. 3, pp. 299–350, 1998.
[28] J. Møller, A. R. Syversveen, and R. P. Waagepetersen, "Log Gaussian Cox processes," *Scandin. J. Statist.*, vol. 25, no. 3, pp. 451–482, 1998.
[29] S. Zhang, S. Zhou, and Z. Niu, "Traffic aware offloading for BS sleeping in heterogeneous networks," in *Proc. Asilomar Conf. Signals, Syst., Comput.*, Nov. 2014, pp. 1933–1938.

SHENG ZHOU (S'06–M'12) received the B.E. and Ph.D. degrees in electronics engineering from Tsinghua University, Beijing, China, in 2005 and 2011, respectively. In 2010, he was a Visiting Student with the Wireless System Laboratory, Department of Electrical Engineering, Stanford University, Stanford, CA, USA. He is currently an Assistant Professor with the Department of Electronic Engineering, Tsinghua University. His research interests include cross-layer design for multiple antenna systems, cooperative transmission in cellular systems, and green wireless communications.

Dr. Zhou co-received the best paper award at the Asia-Pacific Conference on Communication in 2009 and 2013, the 23rd IEEE International Conference on Communication Technology in 2011, and the 25th International Teletraffic Congress in 2013.

DONGHEON LEE received the B.Sc. and M.Sc. degrees in electronics engineering from Pusan National University, Busan, Korea, in 2007 and 2009, respectively, and the Ph.D. degree in electronics engineering from Tsinghua University, Beijing, China, in 2014. He is currently with the Corporate R&D Center, SK Telecom, Korea. His research interests include performance evaluation of wireless cellular networks, teletraffic engineering, green communications, data center networks, SDN, and NFV.

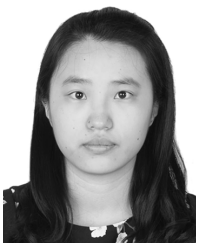

BINGJIE LENG received the B.S. degree in electronics engineering from Tsinghua University, China, in 2014, where she is currently pursuing the master's degree with the Department of Electronic Engineering. Her research interests include infrastructure sharing in cellular networks, cellular big data, and green wireless communications.

XUAN ZHOU received the Ph.D. degree in communication and information systems from Zhejiang University, Hangzhou, China. From 2009 to 2014, he was a System Engineer with China Mobile Zhejiang Company. Since 2014, he has been a Solution Architect with the Service Provider Operation Laboratory, Huawei Technologies. His research efforts focus on innovative service scenarios in 5G and NFV/SDN.

HONGGANG ZHANG (M'01–SM'11) was the International Chair Professor of Excellence with the Université Européenne de Bretagne and Supélec, France. He is currently a Full Professor with the College of Information Science and Electronic Engineering, Zhejiang University, Hangzhou, China. He is an Honorary Visiting Professor with the University of York, York, U.K. He is active in research on green communications, and was a leading Guest Editor of the *IEEE Communications Magazine* of the Special Issues on Green Communications. He has co-authored and edited two books entitled *Regulatory Policy and Economics, Implementation* (John Wiley & Sons) and *Green Communications: Theoretical Fundamentals, Algorithms and Applications* (CRC Press), respectively, with the titles of Cognitive Communications-Distributed Artificial Intelligence. He takes the role of Associate Editor-in-Chief of *China Communications* and Series Editor of the *IEEE Communications Magazine* for its Green Communications and Computing Networks Series. He served as the Chair of the Technical Committee on Cognitive Networks of the IEEE Communications Society from 2011 to 2012.

ZHISHENG NIU (M'98–SM'99–F'12) received the degree from Beijing Jiaotong University, China, in 1985, and the M.E. and D.E. degrees from the Toyohashi University of Technology, Japan, in 1989 and 1992, respectively. From 1992 to 1994, he was with Fujitsu Laboratories Ltd., Japan. He joined Tsinghua University, Beijing, China, in 1994, where he is currently a Professor with the Department of Electronic Engineering. He is also a Guest Chair Professor with Shandong University, China. His major research interests include queuing theory, traffic engineering, mobile Internet, radio resource management of wireless networks, and green communication and networks.

He is a fellow of the Institute of Electronics, Information and Communication Engineers (IEICE). He received the Outstanding Young Researcher Award from the Natural Science Foundation of China in 2009, and the best paper award from the IEEE Communication Society Asia-Pacific Board in 2013. He also co-received the best paper awards from the 13th, 15th, and 19th Asia-Pacific Conference on Communication in 2007, 2009, and 2013, respectively, and the International Conference on Wireless Communications and Signal Processing in 2013, and the Best Student Paper Award from the 25th International Teletraffic Congress. He is the Chief Scientist of the National Basic Research Program (so called 973 Project) of China on Fundamental Research on the Energy and Resource Optimized Hyper-Cellular Mobile Communication System (2012–2016), which is the first national project on green communications in China.

Dr. Niu has been an active volunteer for various academic societies, including the Director of Conference Publications (2010–2011) and the Director of the Asia-Pacific Board (2008–2009) of the IEEE Communication Society, a Membership Development Coordinator of the IEEE Region 10 (2009–2010), a Councilor of IEICE in Japan (2009–2011), and a Council Member of the Chinese Institute of Electronics (2006–2011). He was a Distinguished Lecturer (2012–2015) and the Chair of the Emerging Technology Committee (2014–2015) of the IEEE Communication Society, a Distinguished Lecturer of the IEEE Vehicular Technologies Society (2014–2016), a member of the Fellow Nomination Committee of the IEICE Communication Society (2013–2014), a Standing Committee Member of the Chinese Institute of Communications (CIC) (2012–2016), and an Associate Editor-in-Chief of the *IEEE/CIC China Communications* joint publication.